https://doi.org/10.3311/PPci.36880

Periodica Polytechnica Civil Engineering

The Use of Machine Learning Models and SHAP Interaction Values to Predict the Soil Swelling Index

Myriam Letif[1*], Ramdane Bahar[1], Nourredine Mezouar[2]

[1] LEEGO Laboratory, Department of Geotechnic and Hydraulic, Faculty of Civil Engineering, University of Sciences and Technology Houari Boumediene (USTHB), P. O. B. 32, El-Alia Bab-Ezzouar, 16111 Algiers, Algeria
[2] Département Microzonage Sismique, Centre National de Recherche Appliquée en Génie Parasismique (CGS), Rue Kaddour Rahim, P. O. B. 252, Hussein Dey, 16040 Algiers, Algeria
[*] Corresponding author, e-mail: mletif@usthb.dz

Received: 14 March 2024, Accepted: 20 October 2024, Published online: 04 November 2024

Abstract

Predicting the soil swelling index (C_s) is crucial for geotechnical engineer to ensure the stability of civil engineering conceptions. Recently, ML models has sparked great interest from researchers in predicting the soil swelling index. However, due to the black-box nature of ML models, their prediction capabilities are still uninterpretable. This study aims to predict the soil swelling index using ML algorithms and interpret predictions. First, it employs the prediction capability of the Gaussian process regression (GPR) algorithm and compares it to the artificial neural network (ANN) for prediction the soil swelling index. Second, the SHAP algorithm as one recent explainable artificial intelligence (XAI) models is applied to interpret the predictions of the complex GPR and ANN models. The compiled experimental database covers 362 clayey samples gathered from different sites located in Northern Algeria. The modeling involved six input features, including the liquid limit (*LL*), plastic limit (*PL*), plasticity index (*PI*), water content (ω_n), dry density (γ_d), and void ratio (*e*) to predict the soil swelling index. The findings based on statistical metrics showed a good performance of GPR with R^2 = 0.78 and of ANN with R^2 = 0.79. Comparative study based on Wilcoxon signed- rank test and sign test indicated that the ANN outperform better than GPR. Based on the interpretations obtained by SHAP algorithm, it is observed that the liquid limit (*LL*) and plastic limit (*PL*) are the two main input features that influence the C_s, indicating, the higher content of *LL* and *PL* increase the model's output.

Keywords

soil swelling index, machine learning, Gaussian process regression, artificial neural network, SHAP algorithm

1 Introduction

Swelling soils are widely distributed worldwide, particularly in arid and semi-arid climatic areas and usually remain unsaturated [1, 2]. Extended periods of drought, high temperatures in all seasons, and heavy rainfall can severely harm the hydric cycles of swelling soils. These factors contribute to the variation in the volume of fine-grained soils by shrinkage during drought periods and swelling following precipitation, reflecting the "shrinkage-swelling" phenomenon. This unpredictable behavior can lead to severe damage, such as shifting foundations and cracking walls. As such, it is important to determine the potential risks of shrinkage-swelling soil and understand factors influencing this phenomenon when planning for any civil engineering projects.

The potential of swelling and shrinkage can differ depending on the expansive characteristics of clay minerals, physical properties such consistency limits, clay content (CC), water content (ω_n), void ratio (e), and dry density (γ_d). In-situ conditions can also impact the behavior of expansive soils. A highly consolidated soil is more critical than normally consolidated soil with a comparable void ratio [3–5]. Swelling soil properties have been widely examined by a number of scholars forecasting factors controlling soil swelling behavior under various conditions. Medjnoun et al. [6] conducted a mineralogical and geotechnical characterization study of swelling marly clays in the Medea region, Algeria. They highlighted that water content and density are more influencing factors on the behavior of swelling clays near the surface and less for deeper layers which are less exposed to climatic variations. They also add that the swelling potential decreases when the water content is higher; the increase in water content during imbibition being the triggering factor for swelling.

Cite this article as: Letif, M., Bahar, R., Mezouar, N. "The Use of Machine Learning Models and SHAP Interaction Values to Predict the Soil Swelling Index", Periodica Polytechnica Civil Engineering, 2024. https://doi.org/10.3311/PPci.36880

In practice, soil swelling behavior is characterized by different indices such as swelling index (C_S), Pressure swell (P_S), Free swell (*FS*), and Swelling Potential (*SP*). Oedometer test with incremental loading and Triaxial test are both commonly laboratory tests used to quantify these different soil swelling parameters. These methods have significant advantages, such as a good definition of spatial and temporal boundary conditions, strict control of drainage conditions, and relatively precise identification of soil mechanical properties [7]. However, they are expensive and time-consuming. These limitations are usually overcome by using existing empirical models that predict the soil swelling indices based on different physical soil properties. Countless empirical equations exist in this field. Such techniques are based on conventional statistical modeling which cannot generate the complex behavior of the system, particularly for systems that have nonlinear behavior or interdependency among several variables that control the model's response.

In the era of Industry 4.0, machine learning (ML) algorithms have witnessed an exponential rate of applications in different engineering fields due to their robustness in prediction and classification modeling. ML models utilize algorithms that have the ability to improve their performance without requiring explicit programming or hard coding [8]. ML, as part of an intelligent system in Industry 4.0, can be used for different tasks, such as optimization, quality control, prediction, investigating decision-making, and many others [9]. Different ML models have been applied to predict the potential of soil swelling. In early investigations, Das et al. [10] employed four ML algorithms namely, support vector machines (SVM), Levenberg-Marquardt neural network (LMNN), Bayesian regularization neural network (BRNN), and differential evolution neural network (DENN) to predict swelling potential based on five input parameters. Recently, Ermias and Vishal [11] applied a feed-forward neural network (FFNN) to predict the swelling potential based on six input parameters and compared their results with multiple regression. They concluded that the FFNN model yielded significantly higher prediction accuracy than the multiple regression model. Jalal et al. [12] predicted soil swelling pressure using an artificial neural network (ANN), an adaptive neuro-fuzzy system (ANFIS), and genetic expression programming (GEP) based on nine input parameters. They found that GEP achieved the best prediction accuracy compared to ANN and ANFIS. Eyo et al. [13] employed different intelligent models including ANN, support vector machine (SVM), ANFIS, Bayesian linear regression (BLR), Bayes point machine (BPM), Deep-support vector machine (D-SVM), multiple linear regression (REG), logistic regressor (LR), decision forest (RDF), boosted trees (BDT), voting meta-ensemble (VE), stacking meta-ensemble (SE), based on three different input scenarios. Each scenario includes three input parameters, and they found that that scenario 3-based models (input of Activity, cation exchange capacity, *LL*) give the best accurate results. Dam Nguyen et al. [14] applied three different intelligent models namely, bagging multiple layer perceptron neural network (Bagging-MLP), genetic programming (GP), multilayer perceptron (MLP). They found that the Bagging-MLP yielded high prediction performance in predicting soil swelling potential. Teodosio et al. [8] used a deep learning model to forecast the shrink-swell index based on two different combinations of soil properties. The first combination includes four input parameters, namely, liquid limit (*LL*), plastic limit (*PL*), plasticity index (*PI*), and linear shrinkage (*LS*), while the second combination adds the fines per cent. They concluded that the model that combines all input parameters, i.e., the second scenario, performs best in predicting the shrink-swell index. Narmandakh et al. [5] provided two types of neural networks namely, the feed-forward neural network (FFNN) and the cascade-forward neural network (CFNN). They found that the predictive modeling by FFNN showed substantial improvement compared to previous empirical and semi-empirical relations in predicting soil swelling potential. Taherdangkoo et al. [15] predicted the swelling pressure using an FFNN trained with Levenberg–Marquardt, Bayesian regularization, scaled conjugate gradient, and genetic algorithm. Lately, Jalal et al. [16] integrated the ANN with four metaheuristic algorithms, namely, particle swarm optimization (PSO), grey wolf optimization (GWO), slime mold algorithm (SMO), marine predators algorithm (MPO) to predict the swell pressure based on nine input parameters.

Despite the higher accuracy performance of the different ML models mentioned above and many others, they are categorized as "black-box" models. That is, they offer only the final output with no information related to the relationship between inputs and output; therefore, the output of ML models is still uninterpretable [17]. To alleviate this shortcoming, a novel field, known as explainable artificial intelligence (XAI), has emerged to allow applicants to understand complex ML models' output [18]. A Shapely value for machine learning algorithm, is one XAI-based

algorithm that allow to understand the influence of input variables on the ML models' output. Recently, the SHAP algorithm has witnessed, different applications in civil engineering like construction materials [19–22]. In geotechnical engineering, a growing number of studies have started to utilize SHAP. Kannangara et al. [17] used the SHAP algorithm to explain the model output of the random forest (RF) algorithm in predicting shield tunneling-induced settlement. Kim et al. [23] applied SHAP to investigate the contribution of input variables to the model output of the extreme gradient boosting (XGboost) ML algorithm for predicting undrained shear Strength. Jas and Dodagoudar [24] employed SHAP to explain the model output of the XGboost ML algorithm for assessing soil liquefaction potential. Karakaş et al. [25] applied SHAP to evaluate the model output of ML algorithms for predicting the ultimate bearing capacity of piles. Swarnkar et al. [26] explained the ANN model output for predicting the settlement of the ring foundation. Ye et al. [27] predicted the soil compression coefficient using the XGboost, RF, and Bayes algorithms and interpreted their predictions using the SHAP algorithm. Utkarsh and Jain [28] applied the SHAP algorithm to interpret the output of optimized XGboost with the grey wolf algorithm in predicting the swelling pressure of bentonite. While a relatively large amount of research in the literature deals with the application of SHAP in the geotechnical field, the literature that deals with the applications of SHAP for interpreting the output of an ML-based model in predicting soil swelling index for natural soils has not yet been conducted.

Therefore, the main purpose of this study is to predict the soil swelling index and to interpret the prediction. We use the prediction capability of the Gaussian process regression (GPR) and compare it to ANN in predicting the soil swelling index. Afterward, The SHAP algorithm is applied to interpret the predictions of soil swelling index generated by GPR and ANN models. For the first time, this study is going to investigate the combination of SHAP-GPR and SHAP-ANN systems in the prediction of soil swelling index.

2 Background of the algorithm used

2.1 Gaussian process regression (GPR)

GPR is a non-parametric probabilistic machine learning approach based on Bayesian theory and statistical learning theory. Compared to the popular ML techniques such ANN and SVM which are solely based on historical statistical data for training, GPR exploits the advantages of both methods in the sense that it uses both historical data and data fitting approaches to build a robust model [29, 30].

In GPR, the prediction function that relate the input feature set data to the output data with noisy is given in Eq. (1) [31]:

$$Y = f(X) + \xi \,. \tag{1}$$

Where, Y is the observed target values, $f(X)$ is an underlying function. The ξ is noisy term which is assumed to follow a Gaussian distribution with the mean of 0 and the variance ($\xi \sim N(0, \sigma_n^2)$) in GPR. Then priori distribution of the observation Y and the joint prior distribution of the observed value Y and the predicted value y can be obtained [31]:

$$Y \sim N\left(0, \boldsymbol{K}(\boldsymbol{X}, \boldsymbol{X}) + \sigma_n^2 I_n\right) \tag{2}$$

$$\begin{bmatrix} Y \\ y \end{bmatrix} \sim N\left(0, \begin{bmatrix} \boldsymbol{K}(\boldsymbol{X}, \boldsymbol{X}) + \sigma_n^2 I_n & \boldsymbol{K}(\boldsymbol{x}_*, \boldsymbol{X}) \\ \boldsymbol{K}(\boldsymbol{x}_*, \boldsymbol{X}) & \boldsymbol{K}(\boldsymbol{x}_*, \boldsymbol{x}_*) \end{bmatrix}\right) = N\left(0, \begin{bmatrix} K & K_*^{\mathrm{T}} \\ K_* & K_{**} \end{bmatrix}\right) . \tag{3}$$

Where $\boldsymbol{K}(\boldsymbol{X}, \boldsymbol{X}) = (\kappa_{ij})$ is a symmetric positive definite covariance matrix, whose element measures the correlation between x_i and x_j using a kernel function κ. $\boldsymbol{K}(\boldsymbol{X}_*, \boldsymbol{X}) = \boldsymbol{K}(\boldsymbol{X}, \boldsymbol{X}_*)^{\mathrm{T}}$ is the covariance between the test set X_* and training set X. $\boldsymbol{K}(\boldsymbol{X}_*, \boldsymbol{X}_*)$ is the covariance matrix of the test set itself. I_n is a n-dimensional unit matrix [31]. The common kernel functions are: squared exponential kernel, Matern kernel 5/2, Matern kernel 3/2. The kernel functions are parameterized by a set of kernel hyper-parameters defined as: length-scale, signal variance, and noise variance [32]. These parameters are usually assumed to be unknown but rather are learned from the data [32].

2.2 Artificial neural network (ANN)

ANNs are one well-known ML algorithms inspired by the biological human brain. They consist of several interconnected parallel neurons capable of transferring the information pertaining to the data processing.

ANNs typically consist of three layers: input, hidden, and output. Each layer includes a certain number of neurons. In the input layer, the neurons correspond to the input variables, while the last layer corresponds to the output variable. As for the hidden layer, the researcher can face the following two problems. The first is "how to set the

number of hidden layers?" and the second is "how to set the number of hidden neurons?". Both settings depend on the problem approximation. Usually, trial-and-error approach is common method employed in fixing the number of hidden nodes, because there is no general rule in selecting the number of hidden neurons [33, 34]. In the case of hidden layers, several studies reported that an ANN with single hidden layer containing a finite number of neurons is capable of approximating any non-linear problem.

In ANN, the correlation between input parameters with target value(s) is conducted through learning process. Throughout the training phase, the system diligently focuses on enhancing its precision and efficiency by minimizing error on the training patterns. Then, the validation of the trained model is tested using another dataset. The mode treatment of the input dataset in the multi-layer perceptron network can be represented mathematically in Eq. (4) [35, 36]:

$$Y_j = f\left[\theta_j + \sum_{i=1}^{N}\left(w_{ij}X_i\right)\right]. \quad (4)$$

Where, θ_j is the bias at the hidden layer; w_{ij} is the connection weights between the input variable and hidden layer; X_i is the input variable; Y_j is the output variable; f is the transfer function; and N is the number of hidden neurons [34].

2.3 SHAP algorithm

The SHAP method based on game theory, reflects the strategies that can interpret the ML-based models. The Shapely value for a specific input variable j (φ_j) is the average marginal contribution of an input variable j for all subsets (S) of input variables (N), without containing input variable j, as expressed as follows Eq. (5) [17]:

$$\varphi_j = \sum_{S\subseteq\mathcal{M}\setminus\{j\}} \frac{|S|!(M-|S|-1)!}{M!}\left(f\left(S\cup\{j\}\right)-f(S)\right), \quad (5)$$
$$j = 1,\ldots M.$$

Where f is the original of prediction model, $\mathcal{M}$ is set of all features, M is the total of number of input variables, j is specific value of the j^{th} variable, and S is a subset of features.

In SHAP, output of the prediction model for single observations is explained by linear function as follows Eq. (6) [17]:

$$g(x') = \phi_0 + \sum_{j=1}^{M}\phi_j x'_j = f(x). \quad (6)$$

Where $g(x')$ means the explainable model with simplified input simplified input x'; $f(x)$ is the ML model with the original input variables x; ϕ_0 is the constant value when all inputs are missing, M is the total of number of input variables, j is specific value of the j^{th} variable.

3 Data collection and statistical analysis

This research acquired a sufficiently large dataset comprising experimental oedometer test results with other physical soil properties of various clayey soils obtained as consequence of extensive geotechnical investigations in Northern Algeria. There were 362 soil samples, from which samples of 5 different soil types, including clay, silty clay, sandy clay, marly clay and gravely clay, were gathered and tested. These data were collected from different geotechnical laboratories that employed the standard soil testing techniques and followed recommended procedures to determine the swelling index of the soil samples.

In ML terminology, independent variables are usually known as features, and the output variable in known as target [17]. In this study, physical soil properties including liquid limit (*LL*), plastic limit (*PL*), plasticity index (*PI*), dry density (γ_d), water content (ω_n), and void ratio (e) were used as input features to predict swelling soil index. Table 1 presents the statistical description of the basic relevant features of the input and predicted variable, specifying maximum, minimum, mean, and standard deviation error (STD.E). This table shows that the soil swelling index of the collected datasets ranges from 1% to 13.6%, indicating a wide coverage of swelling index ranging from low to high soil's swelling clays. The values of liquid limit (*LL*) and plasticity index (*PI*) both depict a wide span of soil's consistency ranging from low to high clayey soils (CL-CH). It is important to note that the datasets presented in this study did not contain any missing values, presenting a clean dataset for developing ML models. The distribution of input and target variables is shown in Fig. 1. Fig. 1 represents the box plot for input features and the target.

Further statistical analyses were conducted to analyze the interdependence between input features and the target

Table 1 Statistical descriptive for input features and target

Variables	Units	Max	Min	Mean	STD.E
LL		63.48	28	46.17	6.36
PL		31.23	14	22.60	3.19
PI		37.10	11.40	23.56	4.60
γ_d	kN/m^3	19.8	11.0	16.7	1.1
ω_n		34.0	10.98	20.68	4.13
e		0.940	0.290	0.63	0.11
C_S		0.136	0.010	0.040	0.02

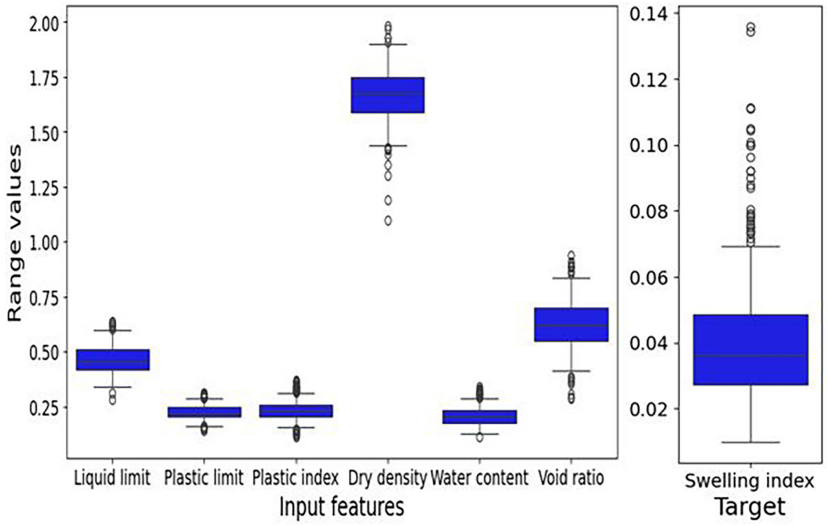

Fig. 1 Box plot for input features and target

variable. The results of Spearman's coefficient matrix are presented in Fig. 2. In Fig. 2, it can be seen that the C_S correlated well with *LL* ($r = 0.67$) and *PI* ($r = 0.62$). It can be seen also that there is weak inverse correlation with dry density ($r = -0.16$). This correlation matrix depicts no multicollinearity problem between variables (i.e., $r > 0.90$) and all parameters are suitable for modeling.

4 Methodology

The modeling methodology used in this study consists of four main steps, as presented in Fig. 3.

Step 1: Database collection. This step involves collecting the whole dataset, including the input features and target.

Step 2: Data wrangling and optimization. The dataset gathered from different national laboratories underwent a meticulous process of transformation aimed at structuring, normalizing, and cleaning to eliminate any errors or irrelevant information from the datasets to present a sufficient quality and consistent dataset for the subsequent training and validating ML models. We employed different

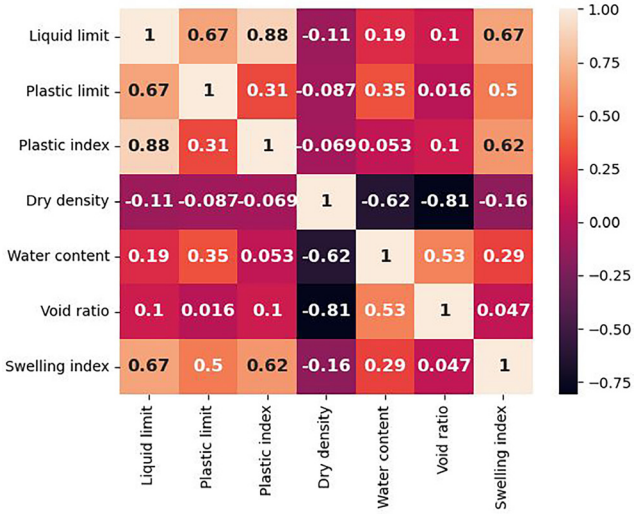

Fig. 2 Heat map of Spearman's correlation coefficient for the input features

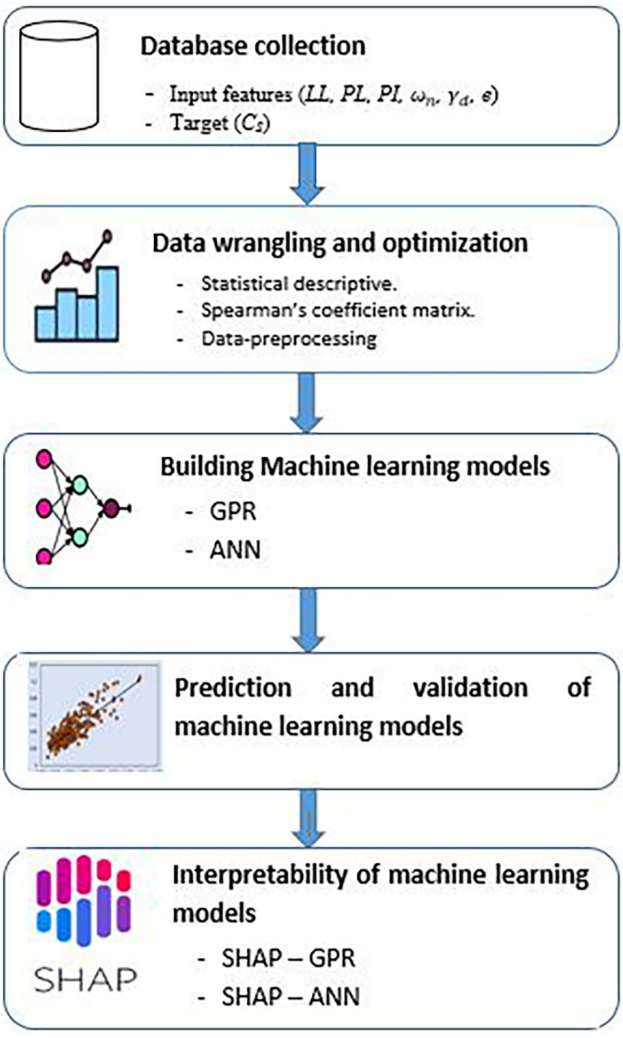

Fig. 3 Methodology flowchart of the proposed study

statistical tools including data distribution analysis, statistical descriptive, and Spearman's coefficient matrix.

In addition, data normalization is conducted to transform the data into a coherent database by removing the overflow due to large or small weights. In this study, the Z-score transformation was adopted using the following mathematical expression Eq. (7):

$$x_i = \frac{X_i - \text{mean}(X_i)}{std(X_i)}. \quad (7)$$

Where x_i is the normalized value of X_i, mean(X_i) and $std(X_i)$ are the mean and standard deviation of measured values, respectively. Following that, the entire data was split into equal-sized *k*-subsets using the *k*-fold cross-validation (KFCV) method, where each K-1 fold subset is used for testing and the remain for training the AI model. The choice of K number division depends on the prediction accuracy quality reached during the validation phase. After several evaluations on the selection of K number fold, this study adopts 10-fold CV subsets.

Step 3: Building of machine learning models. In this step, data from training dataset were used to train and construct GPR and ANN models. The GPR was trained using "Matern 3/2" kernel function, "constant" basis function, and Exact GPR fit method. ANN was trained using the Levenberg-Marquardt backpropagation and tang-sigmoid activation function. Besides, we set up, a three-layer network comprising 6 neurons in input layer, 34 hidden nodes in the hidden layer, and one neuron in the output layer. It should note that the 34 hidden neurons were found after a series of trial error analysis, ranging the number of hidden nodes from 5 to 40. Table 2 summarizes the detailed optimized parameter setting for GPR and ANN models for predicting soil swelling index (C_S).

Step 4: Prediction and validation of machine learning models. In this step, we employ three well-known statistical metrics including coefficient of determination (*R*), mean square error (MSE), and mean bias error (MBE) to validate the prediction of ANN and GPR models.

Step 5: Interpretability of machine learning models. In this step, the SHAP algorithm is integrated into GPR and ANN models to interpret the prediction of their output results.

Table 2 An overview of GPR and ANN parameter setting

Model	Parameter	Option/value
GPR	Kernel function (Form of the covariance function)	Matern 3/2
	Basis function (Explicit basis in the GPR)	Constant
	Fit method (Method to estimate parameters of the GPR model)	Exact Gaussian process regression
	Beta (Initial value of the coefficients for the explicit basis)	0.514
	Sigma (Initial value for the noise standard deviation of the Gaussian process model)	0.619
ANN	Number of layers	3
	Activation function	tang-sigmoid function
	Training algorithm	Levenberg-Marquardt backpropagation
	Number of neurons	Input layer: 6 Hidden layer: 5–40 Output layer: 1
	Learner rate	0.0001
	Number of iterative learning	20

5 Results

5.1 Prediction

In this subsection, the results of the developed GPR and ANN are presented and discussed. The performance of each model was achieved using coefficient of determination (*R*), mean square error (MSE), and mean bias error (MBE). The *R* value detect the relative correlation between measured and predicted values. Higher *R* is good performance, lower *R* is worst results. Smith [37] recommended that for $R > 0.8$, the relationship depict a strong result, for $R < 0.2$, it indicates a weak performance, and for $0.2 < R < 0.8$, the model is acceptable. MSE and MBE aim to compute the error of a given network. The lower MSE and MBE the better model calibration.

Regression plots of predicted soil swelling index values in function of the corresponding measured values using training datasets and testing data sets are illustrated in Figs. 4 and 5, for training and testing phases, respectively. The solid line (blue line) represents the trend line generated in each case to estimate the correlation of the results i.e. slope and intercept. The closeness of this line to the dotted line ($Y = T$) indicates the accuracy of the developed model, while the farther one means an increase in error and, therefore, a less accurate model. The linear fit equation for the training dataset is drawn with slope of 0.81 and 0.62 for ANN and GPR models related to an angle between the trend line (blue line) and the horizontal line of 39° and 32°, respectively. The ANN model has the linear fit line closet to the dotted line, which is consist with $R = 0.911$. However, the GPR model produced a lower accuracy compared to ANN model in terms of slope line and coefficient of determination.

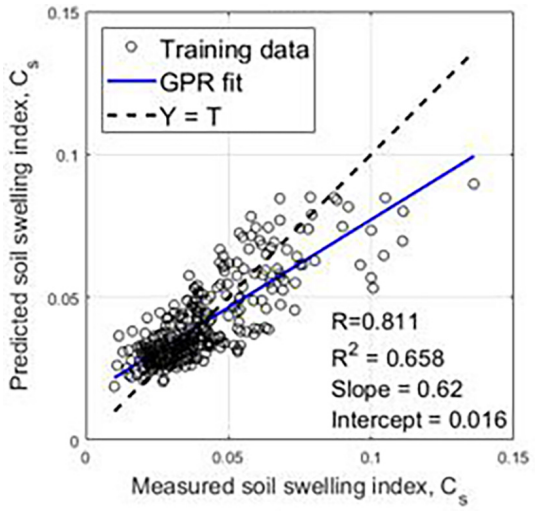

(a)

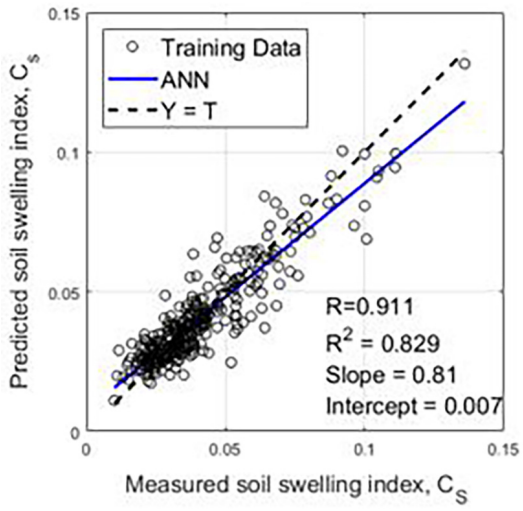

(b)

Fig. 4 Predicted versus measured C_S during training phase for (a) GPR and (b) ANN

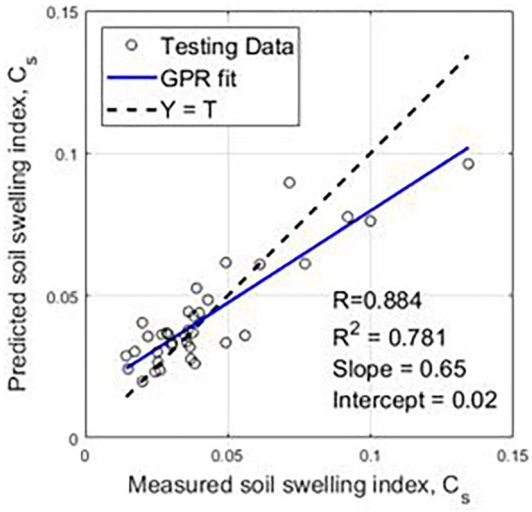

(a)

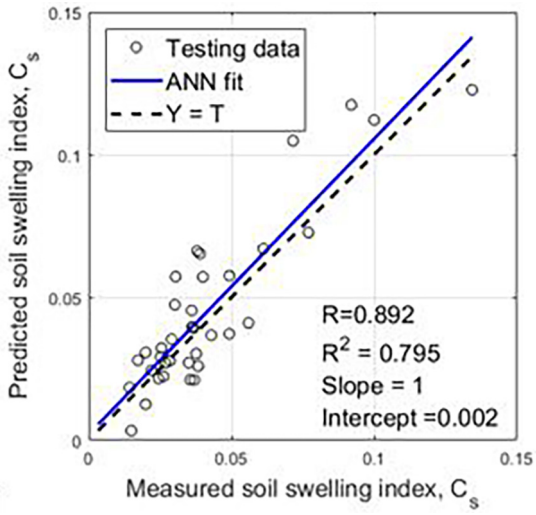

(b)

Fig. 5 Predicted versus measured C_S during training phase for (a) GPR and (b) ANN

For the testing part, the linear fit equation of ANN and GPR had a slope of 1 and 0.65 corresponding to an angle of 45° and 33°, respectively. It indicates that the ANN model has the best fit, which is similar to the dotted line forming an angle of 45°. This is consistent with $R^2 = 0.795$. The GPR model shows weak slope results but performs better in coefficient determination ($R^2 = 0.781$).

ANN depicts a good accuracy performance during training and testing phases according to R^2 despite the complexity of datasets, while GPR shows weak results compared to ANN.

In terms of error measurements, during training phase, ANN has produced a MSE and MBE of 0.0001 and 0.01, respectively, and GPR has achieved a MSE and MBE 0.0001 and 0.03, respectively. During testing phase, ANN has produced a MSE and MBE of 0.0001 and 0.01, respectively, and GPR has achieved a MSE and MBE 0.0002 and 0.01, respectively. These results indicate that ANN produced a lower error during the training and testing phases than GPR and is adequate with R^2.

5.2 Comparison of predictive accuracy

Considering the results of statistical metrics produced for ANN and GPR models. It is no simple to decide on which of these techniques perform better than others. Consequently, two statistical tests, namely the Sign test, and the Wilcoxon Signed-Rank test, are applied to compare the overall effectiveness of each model and make informed decisions on which ML approach is most effective for predicting the soil swelling index. A Wilcoxon Signed-Rank and Sign values under 0.05 reject the null hypothesis indicating difference in the two compared

models, while values upper 0.05 accept the null hypothesis when there is no difference.

Table 3 summarizes the tests results of the upper two statistical tests with 95% degrees of confidence for GPR and ANN models. Both tests accept the null hypothesis of ANN and GPR models. These results indicate that the prediction performance of ANN and GPR models can be considered to be the same in soil swelling index prediction. Combined with results of the model comparison, we conclude that the performance accuracy of predictive ANN model is an effective ML algorithm in predicting soil swelling index.

5.3 SHAP analysis

The SHAP is new algorithm developed to explain the complex ML models' output using Shapely values. In the present study, SHAP is applied to both GPR and ANN models. Summary plot is a typical global view of the Shapley value results. It indicates the contribution of each input variables on model output. The SHAP summary plot obtained for GPR and ANN model is shown in Fig. 6. In Fig. 6, the horizontal axis represents the SHAP values, and the vertical axis represents the input variables ordered from top to bottom, where the variable with upper mean absolute value of the Shapley values is at the top. The color bar indicates the intensity of SHAP values estimated for each input variable. For instance, reddish points represent the highest value, while bluish points represent the lower Shapley values. Positive and negative SHAP values illustrate increasing and decreasing impact on the model output, respectively.

Table 3 Sign and Wilcoxon signed-rank tests results for GPR and ANN models

Test method	GPR	ANN
Sign test	0.405	0.405
Wilcoxon signed-rank test	0.423	0.285

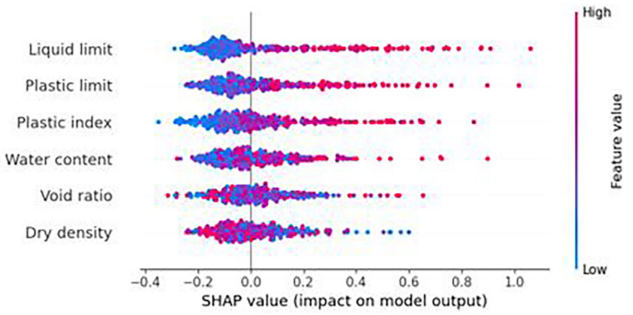

(a)

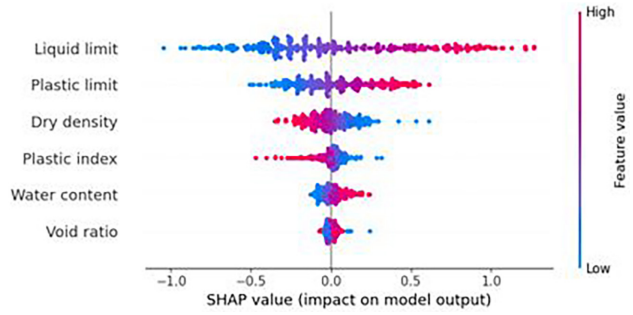

(b)

Fig. 6 Summary plot obtained from SHAP analysis for (a) GPR model and (b) ANN model

According to Fig. 6, the SHAP analysis results of the GPR and ANN models exhibited some common findings. On the one hand, liquid limit (*LL*) and plastic limit (*PL*) are both most input features among the six input features for predicting soil swelling index. The positive and negative SHAP values increase and decrease the model's output, respectively. Accordingly, liquid limit and plastic limit produce positive SHAP values (i.e. positive SHAP values are observed when the liquid limit and plastic limit are large). This makes sense, as higher content of liquid limit and plastic limit increases the soil swelling index. Similarly, for the water content (ω_n), as higher content of this input can lead to increase the soil swelling index. On the other hand, dry density (γ_d) has the negative effect on the soil swelling index, meaning that the soil swelling index decreases as the amount of dry density increases.

Nevertheless, there is certain difference in the SHAP results between the GPR and ANN models. Specifically, with GPR model, the contribution of the input features on soil swelling index in decreasing order was liquid limit (*LL*), plastic limit (*PL*), plasticity index (*PI*), water content (ω_n), void ratio (*e*), and dry density (γ_d). For the ANN model, the input features influence on soil swelling index in decreasing order was liquid limit (*LL*), plastic limit (*PL*), dry density (γ_d), plasticity index (*PI*), water content (ω_n), while void ratio (*e*) have little influence. This means that GPR and ANN models choose differently the importance of input features on predicting soil swelling index. This difference could be mainly related to the ML model's characteristics. Indeed, Salih et al. [38] emphasized that SHAP is a model-dependent method. This means that SHAP's outcome depends on the model used. Consequently, when different models are applied, the top features SHAP identifies may differ among ML models [38].

Fig. 7 illustrates the relative importance of each input feature according to their mean SHAP values. This graph provides additional information, where the features are ordered from the highest to the lowest effect on the prediction. It considers only the absolute SHAP value and does

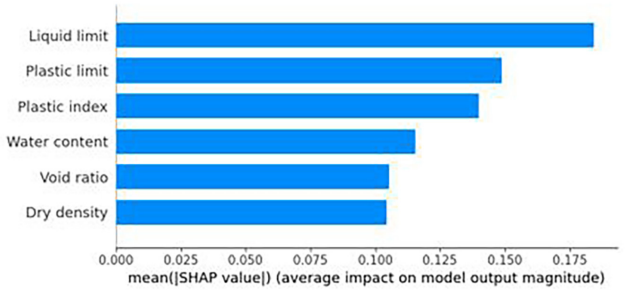

(a)

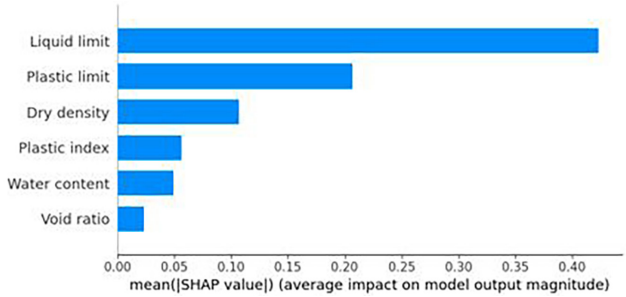

(b)

Fig. 7 Relative importance of each feature obtained from SHAP analysis for (a) GPR model and (b) ANN model

not consider whether the feature affects the prediction in a positive or negative way. Maximum mean |SHAP| values calculated by ANN and GPR reached 0.45 and 0.18, respectively. These values are related to liquid limit (LL) feature. The minimum mean |SHAP| values calculated by ANN and GPR reached 0.01 and 0.10, corresponding to void ratio (e) and dry density (γ_d), respectively.

6 Discussion

This study compared the predictive ability of the developed ANN and GPR with Işık [39], Alptekin and Taga [40], and Abdulkareem and Aziz [41] empirical correlations. The comparative study used the coefficient of determination (R^2), the root means square error (RMSE), and the slope of linear fit for each model.

Table 4 presents the performance results of each model. It can be observed that the developed ANN model in this study gives accurate results in terms of the slope linear fit equation compared to GPR and previous studies. Considering the coefficient of determination (R^2), the ANN and GPR models showed similar results. The previous empirical models of Işık [39], Alptekin and Taga [40], and Abdulkareem and Aziz [41] that express the soil swelling index based on liquid limit (LL) generated an acceptable R^2. The multiple regression model of Işık [39] generated a weak R^2. In terms of error measurement, as computed by RMSE, the developed model ANN and GPR in this study produced a lower error. Likewise, the empirical model of Işık [39], which used LL as an input feature, generated a lower error compared to the Alptekin and Taga [40] and Abdulkareem and Aziz [41] models. When compared among different empirical models proposed by Işık [39], Alptekin and Taga [40], and Abdulkareem and Aziz [41], it is observed that only equations that express the soil swelling index based on the input feature LL generate acceptable results. The comparative study confirms that the developed ANN model in this study outperforms the previous empirical equations in predicting the soil swelling index.

7 Conclusions

This study aimed to address an important gap in the research literature dealing with soil swelling index prediction using machine learning algorithms. Two ML models namely GPR and ANN were applied to predict the soil swelling index associated to six input features namely,

Table 4 Model comparison of the predictive models

Model name	Model to predict	Slope	R^2	RMSE
Işık [39]	$C_S = 0.0007LL + 0.0062$	0.15	0.60	0.01
	$C_S = (-0.0003 \times \omega_n) - 0.027 \times \gamma_d + 0.06 \times e_0 + 0.037$	0.09	0.08	0.02
Alptekin and Taga [40]	$C_S = (3 \times 10^{-5}) LL^{1.6}$	0.1	0.63	0.04
	$C_S = (0.0009 \times PL) + 0.0013$	0.05	0.23	0.03
	$C_S = 0.0005 \times PI^{1.04}$	0.09	0.49	0.04
Abdulkareem and Aziz [41]	$C_S = 0.002LL + 0.008$	0.43	0.60	0.06
	$C_S = 0.002PI + 0.036$	0.31	0.49	0.04
ANN (current study)	ANN (LL, PL, PI, γ_d, ω_n, and e)	1	0.79	0.01
GPR (current study)	GPR (LL, PL, PI, γ_d, ω_n, and e)	0.65	0.78	0.01

LL, *PL*, *PI*, *DD*, ω_n, and e on total of 362 clayey samples. The trained GPR and ANN models were used subsequently as input to the SHAP algorithm to interpret the predictions generated with GPR and ANN. Based on this study, the main conclusions can be drawn:

- The findings indicated that the GPR model could provide accurate and precise results in predicting soil swelling index.
- Comparative study based on statistical metrics and inferential tests depicted that the ANN model performed better than GPR model.
- The application of SHAP algorithm to the GPR and ANN models to understand those outputs prediction, revealed that the soil swelling index predominantly depends on liquid limit (*LL*) and plastic limit (*PL*). Further, the importance of input variables varies according to the type of ML models.
- Further research should expand the size of database and also input features. In addition, applicants in this area should keep in mind that developed models in this study are valid within the range of database used. Optimized machine learning models using different metaheuristic algorithms are also suggested to predict the soil swelling indices.
- Finally, this study has extended the evolving machine learning applied in geotechnical engineering, specifically in prediction soil swelling index. Up to now, the application of XAI methods in geotechnical engineering is new field and less explored. Based on our results we recommend to apply the similar approach used in this study for solve further geotechnical problems.

Acknowledgment

The authors would like to extend their considerable acknowledgment to the National Earthquake Engineering Research Center (CGS) of Algiers, Algeria and Cosider Travaux Publics for making available the geotechnical data used as a part of this research.

References

[1] Fredlund, D. G., Rahardjo, H. "Soil Mechanics for Unsaturated Soils", John Wiley & Sons, 1993. ISBN 9780471850083

[2] Liang, W., Yan, R., Xu, Y., Zhang, Q., Tian, H., Wei, C. "Swelling pressure of compacted expansive soil over a wide suction range", Applied Clay Science, 203, 106018, 2021. https://doi.org/10.1016/j.clay.2021.106018

[3] Gould, S. J. F., Kodikara, J., Rajeev, P., Zhao, X.-L., Burn, S. "A void ratio–water content–net stress model for environmentally stabilized expansive soils", Canadian Geotechnical Journal, 48(6), pp. 867–877, 2011. https://doi.org/10.1139/t10-108

[4] Teodosio, B., Kristombu Baduge, K. S., Mendis, P. "A review and comparison of design methods for raft substructures on expansive soils", Journal of Building Engineering, 41, 102737, 2021. https://doi.org/10.1016/j.jobe.2021.102737

[5] Narmandakh, D., Butscher, C., Doulati Ardejani, F., Yang, H., Nagel, T., Taherdangkoo, R. "The use of feed-forward and cascade-forward neural networks to determine swelling potential of clayey soils", Computer and Geotechnics, 157, 105319, 2023. https://doi.org/10.1016/j.compgeo.2023.105319

[6] Medjnoun, A., Khiatine, M., Bahar, R. "Caractérisation minéralogique et géotechnique des argiles marneuses gonflantes de la région de Médéa, Algérie" (Mineralogical and geotechnical characterization of swelling marly clays from the Medea region, Algeria), Bulletin of Engineering Geology and the Environment, 73(4), pp. 1259–1272, 2014. (in French) https://doi.org/10.1007/s10064-014-0582-z

[7] Khemissa, M. "Validity Criteria of Oedometric and Triaxial Test Results", Geotechnical and Geological Engineering, 34(4), pp. 1171–1180, 2016. https://doi.org/10.1007/s10706-016-0036-4

[8] Teodosio, B., Wasantha, P. L. P., Yaghoubi, E., Guerrieri, M., C. van Staden, R., Fragomeni, S. "Shrink–swell index prediction through deep learning", Neural Computing and Applications, 35(6), pp. 4569–4586, 2023. https://doi.org/10.1007/s00521-022-07764-7

[9] Bajic, B., Cosic, I., Lazarevic, M., Sremcev, N., Rikalovic, A. "Machine Learning Techniques for Smart Manufacturing: Applications and Challenges in Industry 4.0", In: 9th International Scientific and Expert Conference, Novi Sad, Serbia, 2018, pp. 29–38.

[10] Das, S. K., Samui, P., Sabat, A. K., Sitharam, T. G. "Prediction of swelling pressure of soil using artificial intelligence techniques", Environment Earth Sciences, 61(2), pp. 393–403, 2010. https://doi.org/10.1007/s12665-009-0352-6

[11] Ermias, B., Vishal, V. "Application of artificial intelligence for prediction of swelling potential of clay-rich soils", Geotechnical and Geological Engineering, 38(6), pp. 6189–6205, 2020. https://doi.org/10.1007/s10706-020-01427-x

[12] Jalal, F. E., Xu, Y., Iqbal, M., Javed, M. F., Jamhiri, B. "Predictive modeling of swell-strength of expansive soils using artificial intelligence approaches: ANN, ANFIS and GEP", Journal of Environmental Management, 289, 112420, 2021. https://doi.org/10.1016/j.jenvman.2021.112420

[13] Eyo, E. U., Abbey, S. J., Lawrence, T. T., Tetteh, F. K. "Improved prediction of clay soil expansion using machine learning algorithms and meta-heuristic dichotomous ensemble classifiers", Geoscience Frontiers, 13(1), 101296, 2022. https://doi.org/10.1016/j.gsf.2021.101296

[14] Dam Nguyen, D., Roussis, P. C., Thai Pham, B., Ferentinou, M., Mamou, A., Quang Vu, D., Thi Bui, Q.-A., Kien Trong, D., Asteris, P. G. "Bagging and multilayer perceptron hybrid intelligence models predicting the swelling potential of soil", Transportation Geotechnics, 36, 100797, 2022.
https://doi.org/10.1016/j.trgeo.2022.100797

[15] Taherdangkoo, R., Tyurin, V., Shehab, M., Doulati Ardejani, F., Minh Tang, A., Narmandakh, D., Butscher, C. "An efficient neural network model to determine maximum swelling pressure of clayey soils", Computers and Geotechnics, 162, 105693, 2023.
https://doi.org/10.1016/j.compgeo.2023.105693

[16] Jalal, F. E., Iqbal, M., Khan, W. A., Jamal, A., Onyelowe, K., Lekhraj "ANN-based swarm intelligence for predicting expansive soil swell pressure and compression strength", Scientific Reports, 14(1), 14597, 2024.
https://doi.org/10.1038/s41598-024-65547-7

[17] Kannangara, K. K. P. M., Zhou, W., Ding, Z., Hong, Z. "Investigation of feature contribution to shield tunneling-induced settlement using Shapley additive explanations method", Journal of Rock Mechanics and Geotechnical Engineering, 14(4), pp. 1052–1063, 2022.
https://doi.org/10.1016/j.jrmge.2022.01.002

[18] Linardatos, P., Papastefanopoulos, V., Kotsiantis, S. "Explainable AI: A review of machine learning interpretability methods", Entropy, 23(1), 18, 2020.
https://doi.org/10.3390/e23010018

[19] Mangalathu, S., Shin, H., Choi, E., Jeon, J.-S. "Explainable machine learning models for punching shear strength estimation of flat slabs without transverse reinforcement", Journal of Building Engineering, 39, 102300, 2021.
https://doi.org/10.1016/j.jobe.2021.102300

[20] Cakiroglu, C., Islam, K., Bekdaş, G., Kim, S., Geem, Z. W. "Interpretable machine learning algorithms to predict the axial capacity of FRP-reinforced concrete columns", Materials, 15(8), 2742, 2022.
https://doi.org/10.3390/ma15082742

[21] Zhang, D., Lin, X., Dong, Y., Yu, X. "Machine-Learning-Based uncertainty and sensitivity analysis of Reinforced-Concrete slabs subjected to fire", Structures, 53, pp. 581–594, 2023.
https://doi.org/10.1016/j.istruc.2023.04.030

[22] Haque, M. A., Chen, B., Kashem, A., Qureshi, T., Ahmed, A. A. M. "Hybrid intelligence models for compressive strength prediction of MPC composites and parametric analysis with SHAP algorithm", Materials Today Communications, 35, 105547, 2023.
https://doi.org/10.1016/j.mtcomm.2023.105547

[23] Kim, M., Okuyucu, O., Ordu, E., Ordu, S., Arslan, Ö., Ko, J. "Prediction of undrained shear strength by the GMDH-type neural network using SPT-value and soil physical properties", Materials, 15(18), 6385, 2022.
https://doi.org/10.3390/ma15186385

[24] Jas, K., Dodagoudar, G. R. "Explainable machine learning model for liquefaction potential assessment of soils using XGBoost-SHAP", Soil Dynamics and Earthquake Engineering, 165, 107662, 2023.
https://doi.org/10.1016/j.soildyn.2022.107662

[25] Karakaş, S., Taşkın, G., Ülker, M. B. C. "Re-evaluation of machine learning models for predicting ultimate bearing capacity of piles through SHAP and Joint Shapley methods", Neural Computing and Applications, 36(2), pp. 697–715, 2024.
https://doi.org/10.1007/s00521-023-09053-3

[26] Swarnkar, D. C., Singh, A. K., Shubham, K. "Application of ANN for prediction of settlement of ring foundation", Signal, Image and Video Processing, 2024.
https://doi.org/10.1007/s11760-024-03363-2

[27] Ye, C., Sun, H., Niu, F. "Prediction of Compression Coefficients Based on Machine Learning: A Case of Offshore Wind Farm Site", Iranian Journal of Science and Technology, Transactions of Civil Engineering, 2024.
https://doi.org/10.1007/s40996-024-01464-z

[28] Utkarsh, Jain, P. K. "Predicting bentonite swelling pressure: optimized XGBoost versus neural networks", Scientific Reports, 14(1), 17533, 2024.
https://doi.org/10.1038/s41598-024-68038-x

[29] Al-Homoud, M. S. "Computer-aided building energy analysis techniques", Building and Environment, 36(4), pp. 421–433, 2001.
https://doi.org/10.1016/S0360-1323(00)00026-3

[30] Najibi, F., Apostolopoulou, D., Alonso, E. "Enhanced performance Gaussian process regression for probabilistic short-term solar output forecast", International Journal of Electrical Power & Energy Systems, 130, 106916, 2021.
https://doi.org/10.1016/j.ijepes.2021.106916

[31] Zhang, Z., Ye, L., Qin, H., Liu, Y., Wang, C., Yu, X., Yin, X., Li, J. "Wind speed prediction method using shared weight long short-term memory network and Gaussian process regression", Applied energy, 247, pp. 270–284, 2019.
https://doi.org/10.1016/j.apenergy.2019.04.047

[32] Mahmoodzadeh, A., Mohammadi, M., Ibrahim, H. H., Ahmed Rashid, T., Aldalwie, A. H. M., Ali, H. F. H., Daraei, A. "Tunnel geomechanical parameters prediction using Gaussian process regression", Machine Learning with Applications, 3, 100020, 2021.
https://doi.org/10.1016/j.mlwa.2021.100020

[33] Rafiq, M. Y., Bugmann, G., Easterbrook, D. J. "Neural network design for engineering applications", Computers & Structures, 79(17), pp. 1541–1552, 2001.
https://doi.org/10.1016/S0045-7949(01)00039-6

[34] Lawal, A. I., Kwon, S. "Application of artificial intelligence to rock mechanics: An overview", Journal of Rock Mechanics and Geotechnical Engineering, 13(1), pp. 248–266, 2021.
https://doi.org/10.1016/j.jrmge.2020.05.010

[35] Shahin, M. A., Jaksa, M. B., Maier, H. R. "Recent advances and future challenges for artificial neural systems in geotechnical engineering applications", Advances in Artificial Neural Systems, 2009, 308239, 2009.
https://doi.org/10.1155/2009/308239

[36] Lawal, A. I., Idris, M. A. "An artificial neural network-based mathematical model for the prediction of blast-induced ground vibrations", International Journal of Environmental Studies, 77(2), pp. 318–334, 2020.
https://doi.org/10.1080/00207233.2019.1662186

[37] Smith, G. N. "Probability and statistics in civil engineering: An introduction", Collins, 1986. ISBN 9780003831542

[38] Salih, A., Raisi-Estabragh, Z., Galazzo, I. B., Radeva, P., Petersen, S. E., Menegaz, G., Lekadir, K. "Commentary on explainable artificial intelligence methods: SHAP and LIME", [preprint] arXiv, arXiv:2305.02012v2, 08 May 2023. https://doi.org/10.48550/arXiv.2305.02012

[39] Işık, N. S. "Estimation of swell index of fine grained soils using regression equations and artificial neural networks", Scientific Research and Essay, 4(10), pp. 1047–1056, 2009. https://doi.org/10.5897/SRE.9000461

[40] Alptekin, A., Taga, H. "Prediction of compression and swelling index parameters of quaternary sediments from index tests at Mersin District", Open Geosciences, 11(1), pp. 482–491, 2019. https://doi.org/10.1515/geo-2019-0038

[41] Abdulkareem, A. H., Aziz, D. O. "Multiple regression and ANN (MLP) model for predicting swelling index of Ramadi cohesive soil", IOP Conference Series: Materials Science and Engineering, 737(1), 012116, 2020. https://doi.org/10.1088/1757-899X/737/1/012116